Journal of Materials Chemistry A

Accepted Manuscript

ROYAL SOCIETY OF CHEMISTRY

www.rsc.org/materialsA

Synthesis of Analogous Urchined Rutile Titania Carbon Nanocomposites by Iron-facilitated Phase Transformation of MXene for Environmental Remediation

Guodong Zou[1], Jianxin Guo[1,2], Qiuming Peng[1,], Aiguo Zhou[3], Qingrui Zhang[4,]* and Baozhong Liu[3]*

[1]State Key Laboratory of Metastable Materials Science and Technology, Yanshan University, Qinhuangdao, 066004, PR. China,

[2] Hebei Provincial Key Lab of Optoelectronic Information Materials, College of Physics Science and Technology, Hebei University, Baoding, 071002, PR China

[3]School of Materials Science and Engineering, Henan Polytechnic University, Jiaozuo, 454000, PR. China

[4]Hebei Key Laboratory of Applied Chemistry, School of Environmental and Chemical Engineering, Yanshan University, Qinhuangdao, 066004, PR. China,

*Corresponding email: pengqiuming@gmail.com, zhangqr@ysu.edu.cn

Abstract: Self-assembling has been confirmed as an effective pathway to achieve some unique properties. The recently developed two-dimensional transition metal carbides (termed MXene) provide more potential opportunities to modify the surfaces of layered materials relative to simple graphene. Here we describe one-step method for preparing an analogous urchined rutile TiO_2-C (u-RTC) nano-composite with a high amount of (110) facets by in-situ phase transformation of MXene ($Ti_3C_2(OH)_{0.8}F_{1.2}$) in $FeCl_3$ condition. A layered anatase TiO_2-C (l-ATC) nano-composite with a high percentage of (001) facets forms firstly, then it changes into u-RTC due to the Fe(III) ion induction. The u-RTC displays a high Cr(VI) adsorption capacity of ~225 mg/g, which is higher than the primitive MXene (~62 mg/g) and the l-ATC precursor (~11 mg/g), owing to the inhibition of H_2O molecule adsorption by bridging oxo groups in terms of the first principles calculations. Apart from the fact that the finding confers a desirable aligned oxide-carbon material, this approach may set up a new trajectory to self-assemble functional surfaces of other MXene derivatives.

KEYWORDS: MXene; Two-dimension; Phase transformation; Environmental remediation

The stability and reactivity of inorganic crystals are dominated by their surface chemistry, in which the equilibrium morphology is critical for the synthesis of inorganic crytstals with high reactivity. [1] Achievement of a variety of TiO_2 semiconductors has attracted much attention because of their potential applications for novel photocatalysts, [2-5] energy generation and storage [6, 7] and environmental remediation. [8] Especailly, TiO_2, as a nontoxic material, possesses high concentration of hydroxyl groups on the surface. Whereafter, the pollutants in water can be adsorbed on TiO_2 surface by interacting with the hydroxyl groups. [9-11] As summarized in Table S1, the TiO_2 nanoparticles show a high Cr(VI) adsorption capacity of 3.5-1000 mg/g with the photo-catalytic removal mechanism. However, providing that the reaction is performed in the conditions without photo-catalytic reduction, the adsorption capacity of TiO_2 nanoparticle merely lies in the range of 4.8-63.5 mg/g. Therefore, from a practical point of view, the application of such nanoparticles for wastewater treatment still meets two major drawbacks. Specifically, pure TiO_2 nanoparticles show lower removal efficiencies and weaker reproducibility due to the problem of self-aggregation,[12] causing serious fast diminishment of the active surface area. [9] Additionally, the larger adsorption capcacity without the assistance of photocatalytic reduction is desirable to further extend its application range. [10] To overcome these shortcomings, an approach that TiO_2 nanoparticles are supported by the materials such as activated carbon,[13] glass [14] and ceramics [15] has been attempted, which can improve the stability of TiO_2, reduce the agglomeration of TiO_2, and allow the easy separation from the solution for reuse.

Recently, a large family of 2D materials, labeled MXene, [16-18] has attracted research enthusiasm due to their hydrophilic surfaces, layered structures and good chemical stabilities, excellent electrical conductivities and environment-friendly characteristics. Particularly, a new mild

Al-removing method by HCl and LiF instead of high concentration HF solution paves an exciting way to exploit these 2D layered MXene materials at large-scale in batteries, catalysis and supercapacitors. [19] It is noteworthy that the exterior of MXene after Al-removing are terminated by OH or F groups, resulting in the formation of Ti-OH or Ti-F bondings. [20] Therefore, a direct and simple applied strategy focuses on the OH or F groups. A high lead adsorption ability has been confirmed by ion exchange of OH groups after alkalination intercalation treatment. [21] Another potential application is related to in-situ synthesize some new 2D layered TiO_2-C derivatives in terms of phase transformation. The in-situ investigation demonstrates its possibility under high temperature treatment of ~450 ℃. [22] Additionally, a new TiO_2 hydrid structure has been reported by thermal decomposition, CO_2 gas environment or hydrothermal treatment, which exhibits good properties as an electrode in lithium ion batteries and catalytic performance. [23, 24]

Noteworthy, in view of the existence of F groups on the surface of MXene, it is possible to in-situ synthesize different orientational TiO_2-C composites by tuning the growth of crystallographic planes, rendering some aligned regular TiO_2 carbon based composites. Solvethermal phase transformation is an alternative, which has at least two industrial advantages in contrast to conventional routes: milder and controlled condition over heating decomposition, more facible and pure separation condition. More importantly, the controllable growth of lattice plane can be readily realized by modifying solvents under the F containing conditions. [25, 26]

Herein, we synthesized a new MXene derivative - analogous urchined 2D TiO_2-C nanomaterial-with a high amount of (110) facets by in-situ solvothermal alchohysis of MXene in $FeCl_3$ solution for the first time. This analogous urchined rutile TiO_2-C (u-RTC) is composed of a rutile TiO_2 nanorod with the length of ~1.5 μm and layered C/TiC , in which the introduction of

iron(III) ions transforms the intermediate product of atatase TiO2-C (1-ATC) into u-RTC, This material has a high Cr(VI) adsorption ability of ~225 mg/g, which is higher than the primitive MXene (~62 mg/g) and the l-ATC precursor (~11 mg/g). To the best of our knowledge, this adsorption capacity is the highest value of TiO_2-based materials based on a simple adsorption mechanism. The Cr(VI) ions were slected as model pollutants, due to its highly toxicity and ubiqutous in various effluent from electroplating, metal finishing, leather tanning and pigments industries. The main stucture maintains stable even after five cycles. The first-principle calculations reveals that the bridging oxo groups effectvely inhibite the adsorption of H_2O molecule, resulting in a high Cr(VI) adsorption capacity.

RESULTS AND DISCUSSION

Preparation of u-RTC

In a standard synthesis of MXene, an addition of Ti_3AlC_2 powders was added into a mixture of LiF+6M HCl solution, and then was heated at 60 ℃ for 48 h. After etching, the resulting sediments were separated and then washed to remove the reaction products. The Al layers were moved and the matrix layered MXene was obtained. Notably, the chemical exfoliation of MXene took place in solutions that contain F ions, which resulted in the surface of MXene being covered by some F groups. A representative exfoliated morphology of layered MXene (**Figure 1a**) was observed by field emission scanning electron microscopy (FESEM). The gap width is ~100±50 nm and the thickness of multiple layers is ~25 nm. The X-ray diffraction (XRD, **Figure S1a**) peak at ~9^o confirms the sheets consist of MXene ($Ti_3C_2(OH)_{0.8}F_{1.2,}$ the ratio of OH/F is confirmed by energy-dispersive X-ray (EDX) spectroscope, **Figure S2**) layers containing OH and F groups,

which is consistent with the previous method by etching in 40% HF solution. [21] Meanwhile, the TiC peaks (~3.9 wt.%) formed during hot pressed sintering remain invariable.

A new analogous urchined structure has been prepared by in-situ decomposition of MXene in a mixing solution containing ethylene glycol (EG), $FeCl_3$ and isopropyl alcohol (IPA) **(Figure 1b-c**). The nanorods are perpendicular to the MXene substrate. The average diameter and length, as determined from FESEM and transmission electron microscopy (TEM) images, are ~180±20 nm and ~1.6±0.2 μm, respectively. The nanorod is single crystalline, as evidenced by the sharp selected area electron diffraction pattern (SAED) of a nanorod examined along the [110] zone axis (**Figure 1d)**. Examination of individual nanorod with high-resolution TEM shows that they are completely crystalline along their entire lengths. A corresponding fast-Fourier transform filtered TEM image of tetragonal atomic arrangement on the (010) surface is shown in **Figure 1e**. Lattice figures with interplanar spacing, d_{101}=4.92±0.02 Å and d_{200}=2.21±0.01 Å, are clearly imaged and are consistent with the rutile phase. [6] In addition, some new C peaks are detected (**Figure 1f**), demonstrating that the primitive 2D MXene in-situ changes to a new layered rutile TiO_2-C/TiC nanocomposite. According to the XRD and FESEM, it establishes that the new structure can be marked as an analogous urchined rutile TiO_2-C/TiC (termed u-RTC).

To elucidate the influencing factors (IPA, EG and $FeCl_3$) on the formation of u-RTC, the phase compositions under different conditions are studied by XRD (**Figure S1**). In the case of the sample containing single IPA solvent, the similar XRD peaks remain even after reacting for 24 h, suggesting the MXene is stable in the isopropyl alcohol (IPA) solution, which is added to strengthen the stabilization effect associated with F adsorption on the surface. [1] However, when EG (~0.5 wt.%) is added, some new peaks of anatase TiO_2 (A-TiO_2) are detected, and the peak at ~9^o weakens

simultaneously. It reveals that the alcohol decomposition of MXene takes place and the surface groups of Ti-OH or Ti-F varies to Ti-O groups (TiO_2). At the beginning of free-$FeCl_3$ alcohol decomposition of MXene (1h, **Figure S3**), some sheet-shaped particles are observed on the surface of primitive substrate. The bright field image of TEM and SAED confirm that each free standing crystal shows single crystal characters. The SAED can be indexed into diffraction spots of the [001] zone. The high-resolution TEM image shows the (200) and (020) atomic planes with *a* lattice spacing of 1.897 Å and an interfacial angle of 90°. A corresponding fast-Fourier transform filtered TEM image of tetragonal atomic arrangement on the (001) surface is shown in **Figure S3c**. The average interfacial angel between two parallel facets and other surrounding facets is ~67.5±0.5° (**Figure S4**), which is consistent with the theoretical value of anatase TiO_2 (A-TiO_2). [3,27] Meanwhile, the XRD pattern (**Figure S1**) matches well the crystal structure of the A-TiO_2 (space group *I*41/*amd*). With increasing the incubating time, both the amount and dimension of A-TiO_2 increase significantly. The whole surface of MXene is covered by cuboid nanosheets after 8 h to form a layered anatase TiO_2/C nano-composite (termed l-ATC). The width and thickness are ~230 nm and ~100 nm (**Figure S5**), respectively. However, as the incubating time is further increased, the dimension of A-TiO_2 hardly increases. The whole structure of primitive MXene dissolves after incubating for 24 h (**Figure S3f**).

The morphology variation and phase composition of MXene during in-situ EG decomposition in $FeCl_3$ medium were confirmed by FESEM (**Figure 2)** and XRD **(Figure S6),** respectively. Compared with the decomposition in free-$FeCl_3$, both nano-scale rectangle sheets (A-TiO_2) and rod-like precipitates (R-TiO_2) are observed on the surface of MXene in the initial stage (1h). For R-TiO_2, the values of average width and aspect ratio are ~50 nm and ~1.8, respectively. With

increasing the incubating time, the amount of fine rectangle nanosheets decreases, whilst the number and length of rod-like precipitates increase. The average values of diameter and length change to ~150±20 nm and 1.1±0.2 μm, respectively. Further increasing the incubating time, the rod-like precipitates vary to needle-like ones. The aspect ratio increases to ~28 monotonously, and the average diameter reduces slightly. The continuous increased aspect ratio and the reduced amount of precipitate show that exterior Ostwald-ripening process plays a dominated role on the in-situ EG decomposition of MXene owing to the Fe ion induction (**Figure 2f**). The minimization of the overall surface energy can be attained preferentially by dissolution and regrowth of monomers with respect to the changed morphology rather than by inter-particular aggregation process. [25, 27] The continuous increased dimension is elucidated with respect to weak solvent confinement, [9] wherein the preferential growth along (110) plane results in the presence of needle-shaped R-TiO_2. Noteworthy, when the temperature is higher than 300 ℃, the A-TiO_2 completely changes into R-TiO_2 and pure u-RTC is achieved (**Figure S6b and S7c**). Moreover, the results in terms of Rietveld refinement show that the phase transformation hardly occurs without Fe addition even 300 ℃ for 24 h. It indicates that the formation of u-RTC nano-composite in alcoholysis of MXene is thermodynamic control, which is consistent with the temperature-dependence in hydrothermal reaction or gas decomposition. [23, 28] The whole reaction process has been shown as following:

$$\text{MXene} \xrightarrow{\text{IPA+EG, } \geq 220^{\circ}\text{C}} \text{l-ATC} \xrightarrow{FeCl_3, \geq 220^{\circ}\text{C}} \text{u-RTC+l-ATC} \xrightarrow{FeCl_3, \geq 300^{\circ}\text{C}} \text{u-RTC} \qquad (1)$$

Unexpectedly, only anatase TiO_2 particles are detected on the surfaces of the free-$FeCl_3$ MXene samples (**Figure S6**). Moreover, the phase transformation hardly occurs in the existence of

$CuCl_2$ or NaCl under the same conditions (**Figure S8**). Comparatively, the phase transformation occurs when the additives of Fe salts (NO_3^-, Br^- and Cl^-) are added. Moreover, the anions also affect the product composition under the same conditions. The order on phase transformation follows as: Cl^-> NO_3^-> Br^-. However, compared with the Fe cation, the roles of anions are weaker, which is neglected here and will be discussed in future. It demonstrates that the existence of Fe(III) ion becomes a main prerequisite to prepare u-RTC.

Compared with other $CuCl_2$ or NaCl salt, the $FeCl_3$ addition retards the diameter growth rate by avoiding the side surface coalescing to form a large sheet. The exact role of $FeCl_3$ in controlling the preferential formation of nano-rod R-TiO_2 is not fully understood, but several explanations are possible: akin to F ion, Cl ion is prone to preferentially adsorb and retard the growth rate of closed (110) surface. [29] Secondly, an addition of salt greatly increases the ionic strength of the growth solution, and higher ionic strength favours the formation of smaller electrostatic screening. [25] Finally, a layer of ions next to the scale particles can act as a diffusion barrier for the nano-sheet growth. [30]

Cr(VI) Adsorption Behavior

To evaluate potential applications of high percentage of single facets, the heavy metal ion adsorption behavior has been investigated. Cr(VI) is a representative toxic heavy metal in waters, which can cause serious heathy threaten even at trace amounts, due to its toxicity and carcinogenicity. However, it is impossible to achieve enhanced trance treatment by conventioanl chemical precipitation due to reaction equilibrium. In present work, Cr(VI) uptaking by as-obtained l-ATC (free-$FeCl_3$, 12 h, 200℃), u-RTC+l-ATC ($FeCl_3$, 24 h, 200℃) and u-RTC ($FeCl_3$, 24 h, 300℃) was performed to evaluate the potential applications, and the primitive MXene was involved

for a reference. The surface becomes vague owing to the adherence of Cr(VI) (**Figure S2**). The u-RTC exhibits more favorable Cr(VI) sequestration than both MXene and l-ATC with the maximum sorption capacity of ~225 mg/g (**Figure 3a**), which is the highest value in terms of a simple adsorption mechanism although it is lower than those of nano-TiO_2 nanoparticles with photocatalytic reduction (**Table S1)**. In contrast, the l-ATC displays a low Cr(VI) adsorption value of ~11 mg/g at the same experimental conditions. Taking into account the similar TiO_2-C chemical composition and different crystalline facets, it is believed that the high concentration of Cr(VI) removal is possibly associated with the presence of (110) facets of rutile TiO_2.

The solution pH effects on Cr(VI) adsorption were also conducted. The resultant u-RTC (**Figure 3b**) exhibits an observed pH-dependent process with the optional pH range of ~3.0-6.0, the sorption preferential tendency can be interpreted by the interaction between species of TiO_2 onto u-RTC and Cr(VI) ions. Cr(VI) species may be present in solution, as chromate (CrO_4^{2-}), hydrochromate ($HCrO_4^-$) at acidic solutions or dichromate ($Cr_2O_7^{2-}$) in alkaline conditions. At low pH surroundings (pH<3), the negatively charged bivalent CrO_4^{2-} will tend to transform into the monovalent $HCrO_4^-$, thus, the protonated Ti-OH_2^+ will display the weak adsorption sequestration. In an alkaline environment, it predominately exists as $Cr_2O_7^{2-}$ and the strong repulsion between deprotonated Ti-O^- and CrO_4^{2-} deceases Cr(VI) removal. In addition, the present high level of OH^- competition is also a major reason for the decreasing Cr(VI) sorption.

Sorption kinetics (**Figure 3c**) demonstrates Cr(VI) uptake onto u-RTC is a two stage adsorption process. The beginning fast adsorption (Cr uptake, 28%) can be achieved within 2 min, and then a plodding sorption stage is detected for approaching the final equilibrium within 120 min (total Cr removal 38%). The fast sorption stage can be ascribed to the urchined nano-rod surface

adsorption onto u-RTC, while the prolonging Cr(VI) adsorption might mainly attribute the inner-layer diffusion process towards the laminar MXene matrix.

Considering for the existence of ubiquitous anions in water/wastewaters, e.g. Cl^-, SO_4^{2-}, NO_3^-, the Cr(VI) sorption competition tests onto u-RTC were further estimated (**Figure 3d**). Inspiringly, u-RTC exhibits excellent Cr(VI) sorption selectivity with various high levels of anion additions expect for phosphate. Such efficient adsorption can be ascribed to the formation of the strong inner-sphere complexation between u-RTC and $Cr_2O_7^{2-}$ ions. [31] X-ray photoelectron spectroscopy (XPS) is ascertained to gain a deeper insight into the possible sorption mechanism. A distinct sharp peaks centred at ~577.0 eV suggests the favorable Cr(VI) adsorption onto u-RTC, [32] while the standard Cr2*p* spectrum from pure $K_2Cr_2O_7$ locates at ~579.45 eV (**Figure 4a-b**). The apparent shifts of ~2.45 eV to a lower energy level indicate the formation of strong complex between Cr and u-RTC. In addition，O1*s* spectra of u-RTC before and after Cr(VI) uptake were concerned. The representative spectrum of O1*s* onto bare u-RTC can be divided into two distinctive O species, corresponding to Ti-O (529.9 eV) and Ti-OH (532.1 eV) with area fractions of 89% and 11% respectively. [33] (**Figure 4c**) A full width at half maximum (FWHM) value is approximate 1.45 eV, In contrast, an obvious peak shifting to higher binding energy is detected in Cr(VI) loaded u-RTC with expanded FWHM value of ~2.42 eV, revealing the generation of a new oxygen-complex species. Therefore, the broad O1*s* spectrum can be envisaged to obtain by two overlapping peaks (**Figure 4d**). The peak A located at ~529.9 eV coincides with O1*s* peak of Ti-O species onto bare u-RTC, while a new emerged peak B of ~531.4 eV can be ascribed to the formation of Ti-O-Cr band and a large energy shift of ~1.5 eV verifies the strong sorption affinity. Moreover, the

decreased Ti-O fractions (32.6%) and the increased Ti-O-Cr species (67.4%) further demonstrate the interactions between Ti-O and Cr(VI) ions.

To appraise the actual applicability onto u-RTC, the synthetic Cr(VI) contaminated water containing high levels of competing anions (Cl^-, NO_3^-, SO_4^{2-}), was selected as feeding solution and the effluent history was shown in **Figure 5.** The analogous u-RTC exhibits efficient Cr(VI) adsorption performance with large treated volumes of 370 Kg waters and 1120 Kg per Kg u-RTC based on the criterion of drinking water (0.01 mg/L, WHO) and wastewater discharge standard (0.1 mg/L, China) respectively. The real wastewater test was also confirmed its potential feasibility for water purification **(Figure S9)**. Besides, the exhausted u-RTC can be readily regenerated by 5% NaOH solution for at least five cycles (**Figure 5**).

Mechanism of Cr(VI) Adsorption

To elucidate the different Cr(VI) adsorption results, the adsorption energies of various Cr(VI) speciation adsorption on different surfaces of A-TiO_2, R-TiO_2 and MXene were calculated by the first principles based on the density functional theory. Cr(VI) is present as oxo-species (CrO_4^{2-}, $HCrO_4^-$, and $Cr_2O_7^{2-}$) in aqueous solutions. [34] The concentration of these different forms depends on pH and Cr(VI) concentration, which can be described by the following equation:

$$2CrO_4^{2-} + 2H^+ \leftrightarrow 2HCrO_4^- \leftrightarrow Cr_2O_7^{2-} + H_2O \qquad (2)$$

Other polyanions is ignored because the processing occurs in strong acidic solutions. [35] Taking into account the experimental and previous models, [36-39] different adsorption structures of H_2CrO_4 and $H_2Cr_2O_7$ were built to represent the three adsorption forms of Cr(VI) (**Figure 6a**) to measure the Cr(VI) adsorption ability of TiO_2, which competed with H_2O adsorption on their surface

(**Figure 6b-d**). The adsorption energy and the formation energy were defined by the following equations:

$$E_{ads} = E_{tot} - E_{sub} - E_{Cr} \quad (3)$$

$$E_f = E'_{tot} + E_{H_2O} - E_{sub} - E_{Cr} \quad (4)$$

where E_{tot}, E_{sub}, and E_{Cr} represent the total energies of product, substrate (TiO_2 or $Ti_3C_2(OH)_2$), and the three forms of Cr(VI) such as H_2CrO_4 and $H_2Cr_2O_7$. E'_{tot} and E_{H_2O} represent the total energy of product and water molecular by chemical reaction. Therefore, when the adsorption energies of Cr(VI) as a certain form such as CrO_4^{2-}, $HCrO_4^-$, and $Cr_2O_7^{2-}$ are lower than that of water molecular on TiO_2 surface, it indicates that the form of Cr(VI) can be adsorption on TiO_2 surface.

According to the definition, we note that all forms of Cr(VI) can adsorb on R-TiO_2 (110) instead of different H_2O molecules (**Figure 7**). The typical electronic local function maps [40] of TiO_2 and H_2CrO_4 interfaces (**Figure S10)** show that the O of H_2CrO_4 bond with Ti atom of TiO_2 surface to strengthen the interaction of H_2CrO_4 and TiO_2 surface. In addition, the H of H_2CrO_4 almost breaks away from H_2CrO_4 to form strong bonding with the O of TiO_2.

Comparatively, the mere CrO_4^{2-} form can adsorb on A-TiO_2 (101) surface. In addition, the surface of A-TiO_2 (001) surface (**Figure 7 and S11**) cannot capture Cr(VI) as the presence of CrO_4^{2-} and $HCrO_4^-$ forms due to the similar adsorption energies with H_2O. Specifically, the predominant completion of H_2O molecules on the surfaces of A-TiO_2 (001) and A-TiO_2 (101) planes results in a low total Cr(VI) adsorption value. In addition, note that the MXene also display a good adsorption ability by electrostatic adsorption and chemical adsorption **(Figure S12**), which is

also confirmed by Ying etc. [41] This discrepancy in adsorption capacity between MXene and R-TiO_2 (110) might partially ascribe to the variation of surface areas.

CONCLUSIONS

This finding offers a new approach for self-assembling some unique properties of two-dimensional materials by a controllable in-situ phase transformation. The chemical exfoliation of MXene generally takes place in the solutions containing F ions, and then the surface of MXene is covered by F groups. Therefore, it satisfies a prerequisite to control the preferential growth of certain lattice planes by tuning the reaction solutions. Depending on this strategy, we successfully prepared a novel two-dimensional materials: an analgous urchined rutile TiO_2-C/TiC with a high amount of (110) facets. The self-assembling two-dimensional Mxene derivative shows outstanding chemical activities in environmental applications. Similar reactions may be used to synthesize a variety of other metallic oxide nanocomposites with respect to more than 60 MXene precursors. We foresee this methodology plays enormous potential roles in exploiting new and unexpected physical and chemical properties of MXene derivatives.

MATERIALS AND METHODS

Synthesis of MXene

The Ti_3AlC_2 powders were made by mixing elemental titanium (Alfa, 99 wt.% purity, particle size < 40 μm), aluminum (Alfa, 99 wt.% purity, particle size < 40 μm) and graphite (Alfa, 99 wt.% purity, particle size < 48 μm) powders in a 3:1.5:2 molar ratio. The powders were ball-milled for 48 h and cold pressed into cylindrical discs (15 mm diameter and 10 mm height) under pressure of 1 GPa. The discs were placed in a tube furnace under flowing argon, and heated to 1450 ℃ for 1 h at a heating rate of 20 K/min. After cooling to room temperature, the discs were then milled for 2 h to

obtain powders for further study (400 mesh).

Concentrated HCl (Fisher, chemical grade), was added to deionized water to prepare a 6 M solution (30 ml). 1.98 g (5 molar equivalents) of LiF (Alfa, 98%) was added to this solution. The mixture was stirred for 5 min with a magnetic Teflon stir bar to dissolve the salt. 3 g Ti_3AlC_2 powders were slowly added over the course of 10 min to avoid initial overheating of the solution owing to the exothermic nature of the reactions. The reaction mixture was then held at 60 ^oC for 48 h, after which the mixture was washed through 5 cycles of distilled water, centrifugation (3,500 rpm, 35 min for each cycle), and decanting, until the supernatant reached a pH of ~6. The Al layer within Ti_3AlC_2 was well exfoliated and the layered MXene ($Ti_3C_2(OH)_{0.8}F_{1.2}$) samples were attached. It is noteworthy that the fluoride addition for Al corrosion will lead to the F coverage onto the surface of MXene, which provides the prerequisite to control the growth of different planes.

***In-situ* Decomposition of MXene.**

Preparation of the u-RTC samples: 0.5 g MXene (MXene was immersed in 25% HF for 24 h at room temperature and dried 100 ^oC for 12 h) and 0, 0.15, 0.3, 0.6 mg $FeCl_3 \cdot 6H_2O$ (Sinopharm Chemical Reagent Co. Ltd , 99 wt.% purity) were mixed with of the mixed 30 mL ethylene glycol and isopropyl alcohol (Sinopharm Chemical Reagent Co. Ltd., 99.7 wt.% purity), wherein the concentration of ethylene glycol is 0.15 ml. The mixture was agitated 3 h on a magnetic stirrer at room temperature and then added into a Teflon-lined stainless steel autoclave with a capacity of 50 ml and kept at 180-300℃ for 4-28 h. After solvothermal (isopropyl alcohol, ethylene glycol and $FeCl_3$) reaction, the grey precipitate was collected, washed with ethanol and distilled water for three times, and then dried in an oven at 80 ℃ for 6 h。

Preparation of the l-ATC sample: 0.5 g MXene (MXene was immersed in 25% HF for 24 h at

room temperature and dried 100 ^{o}C for 12 h) was mixed with 30 mL of the mixed ethylene glycol and isopropyl alcohol (Sinopharm Chemical Reagent Co. Ltd., 99.7 wt.% purity), wherein the concentration of ethylene glycol changes from 0 to 2 vol.%. The mixture was agitated 3 h on a magnetic stir at room temperature and then added into a Teflon-lined stainless steel autoclave with a capacity of 50 ml and kept at 180-300 ℃ for 4-28 h. After solvothermal (alcohol) reaction, the grey precipitate was collected, washed with ethanol and distilled water for three times, and then dried in an oven at 80 ℃ for 6 h.

Structural Characterization.

X-ray diffraction patterns were obtained with a powder diffractometer (Siemens D500, Germany) using Cu Kα radiation (λ = 0.154 nm) and a step scan of 0.02 ^{o}/s. Si powder was added to some samples as an internal standard to calibrate the diffraction angles and the instrumental peak broadening. The results were analysed by Rietveld refinement (using the software Fullprof).

A field emission scanning electron microscope, FESEM (Zeiss Supra 50VP, Germany), was used to obtain high magnification images of the treated samples and conduct elemental analysis via energy-dispersive X-ray (EDX) spectroscope. After sonication, the two-dimensional sheets were investigated by transmission electron microscope, TEM (JEM-2100, Japan), with an accelerating voltage of 200 kV. The TEM samples were prepared by suspending the powders in isopropyl alcohol and placing a drop of the latter on a lacey carbon coated 200 mesh Cu grid.

X-ray photoelectron spectroscopy, XPS, was performed with a spectrometer (ESCALAB-2, Great Britain) equipped with an Mg K_{α} X-ray source (1253.6 eV protons). The Raman spectrometer (Renishaw inVia, UK) was used to characterize the samples. An argon ion laser radiation (515.5 nm) was focused to a spot of ~2 μm using a power of less than 1 mW.

Adsorption Behavior of Chromium

The representative Cr(VI) sequestration is performed by the conventional bottle-point methods. To start the experiments, 0.025 g sorbents of l-ATC in (MXene-IPA)-0.5EG at 200 ℃ for 12 h, u-RTC and l-ATC in (MXene-IPA-0.5EG)-1$FeCl_3$ at 200 ℃ for 24 h, u-RTC in (MXene-IPA-0.5EG)-1$FeCl_3$ at 300 ℃ for 24 h and the primitive MXene were introduced into 50 mL solutions containing a known Cr(VI) contents. Afterward, the above bottles were transferred into an incubator shaker with preferred temperatures for 10-20 h reaction to approach sorption equilibrium. Solution pH can be adjusted using 1% NaOH or 1% HNO_3, if necessary.

Kinetic tests were conducted by introducing 1 g u-RTC sorbent into 500 mL solution containing 15 mg/L Cr(VI) , equipped with a agitating device. The 0.5 mL of solutions were sampled at various time intervals, the sampling time was recorded and the Cr(VI) contents in corresponding samples were assayed by an atomic absorption spectrophotometry.

The common anions, including SO_4^{2-}/Cl^-/NO_3^-/ F^-/PO_4^{3-}, were also added at various levels if necessary; the above bottles are then transferred into a SHZ-85 model incubator shaker with thermostat and shaken under 200 rpm for 24 h at desired temperature to ensure the sorption equilibrium. Finanly, the Cr(VI) concentrations were assayed and the sorption capacities and efficiencies were calculated. The Cr(VI) ions were determined using a Shimadzu AA-6800 atomic absorption/emission spectrometer.

Actual applicability evaluation: 1 g of the prepared u-RTC was introduced into a large bottle containing Cr(VI) ions and the common competing anions. The synthetic Cr(VI) contaminated water was selected as the feeding solution. A peristaltic pump (Lange-580, China) was used to control feeding flow rates and an automatic fraction collector was employed for collecting the

effluent samples at various time intervals. Finally, the Cr(VI) concentration of obtaining effluents were determined as well as their corresponding treated volumes. The exhausted u-RTC can be regerenated by 5% NaOH solution to investigate the repeated properties. Piror to using for repeating adsorption, washing sorbent pH till nertual conditions is necessary.

Computational Details

All calculations are performed based on the density functional theory (DFT), which was implemented in the Vienna ab-initio Simulation Package (VASP) code. [42] The exchange-correlation functional is using the generalized gradient approximation with the Perdue-Burke-Ernzerhof (PBE), [43] and the ion-electron interaction is described with the projector augmented wave (PAW) method. [44] The cutoff energy of plane-wave basis is set at 520 eV. The conjugated gradient method is adopted during geometry optimization, and the criterion of energy convergence is 10^{-6} eV/cell. The Brillouin zone is represented by Monkhorst-Pack with the k-spacing of 0.2 $Å^{-1}$. [45] The smearing width of the partial occupancies, which are determined using the Methfessel-Paxton smearing scheme, [46] is 0.1 eV. A large vacuum space of 20 Å is used for avoid any interaction between layers of TiO_2 and MXene.

ASSOCIATED CONTENT

Supporting Information

Additional figures and table as described in the text. This material is available free of charge via the Internet at http:// pubs.acs.org.

Notes

The authors declare no competing financial interest.

ACKNOWLEDGMENT

We greatly acknowledge the financial supports from NSFC (51422105, 51578476 and 21207112), The Science Foundation for the Excellent Youth Scholars from Universities of Hebei Province (E2015203404, GCC2014058) and Chinese. Heibei Province Technology Foundation for Selected Overseas Chinese, Outstanding Youth Scholar and Youth Top-notch Talent Program. We are grateful to Prof. Hai-Jun Wang in Hebei University for some computation supports with a "Molecule Aggregated Structure" work-station.

REFERENCES

1 Tian N.; Zhou Z.Y.; Sun S.G.; Ding Y.; Wang Z.L. Synthesis of Tetrahexahedral Platinum Nanocrystals with High-Index Facets and High Electro-Oxidation Activity. *Science* 2007;316:732-735.

2 Han X.; Kuang Q.; Jin M.; Xie Z.; Zheng L. Synthesis of Titania Nanosheets with a High Percentage of Exposed (001) Facets and Related Photocatalytic Properties. *J. Am. Chem. Soc.* 2009;131:3152-3153.

3 Yang H.G.; Sun C.H.; Qiao S.Z.; Zou J.; Liu G.; Smith S.C.; Cheng H.M.; Lu G.Q. Anatase TiO_2 Single Crystals with a Large Percentage of Reactive Facets. *Nature* 2008;453:638-641.

4 Greene L.E.; Law M.; Tan D.H.; Montano M.; Goldberger J.; Somorjai G.; Yang P. General Route to Vertical ZnO Nanowire Arrays Using Textured ZnO Seeds. *Nano Lett.* 2005;5:1231-1236.

5 Vayssieres L.; Graetzel M. Highly Ordered SnO_2 Nanorod Arrays from Controlled Aqueous Growth. *Angew. Chem. Int. Ed.* 2004;43:3666-3670.

6 Liu B.; Aydil E.S. Growth of Oriented Single-Crystalline Rutile TiO_2 Nanorods on Transparent Conducting Substrates for Dye-Sensitized Solar Cells. *J. Am. Chem. Soc.* 2009;131:3985-3990.

7 Fujishima A.; Honda K. Electrochemical Photolysis of Water at a Semiconductor Electrode. *Nature* 1972;238:37-38.

8 Tiwari J.N.; Mahesh K.; Le N.H.; Kemp K.C.; Timilsina R.; Tiwari R.N.; Kim K.S. Reduced Graphene Oxide-Based Hydrogels for the Efficient Capture of Dye Pollutants from Aqueous Solutions. *Carbon* 2013;56:173-182.

9 Yang H.G.; Zeng H.C. Synthetic Architectures of $TiO_2/H_2Ti_5O_{11}{\cdot}H_2O$, $ZnO/H_2Ti_5O_{11}{\cdot}H_2O$, $ZnO/TiO_2/H_2Ti_5O_{11}{\cdot}H_2O$, and ZnO/TiO_2 Nanocomposites. *J. Am. Chem. Soc.* 2004;127:270-278.

10 Xing J.; Fang W.Q.; Li Z.; Yang H.G. TiO_2-Coated Ultrathin SnO_2 Nanosheets Used as Photoanodes for Dye-Sensitized Solar Cells with High Efficiency. *Ind. Eng. Chem. Res.* 2012;51:4247-4253.

11 Liu G.; Yang H.G.; Wang X.; Cheng L.; Pan J.; Lu G.Q.; Cheng H. M. Visible Light Responsive Nitrogen Doped Anatase TiO_2 Sheets with Dominant {001} Facets Derived from Tin. *J. Am. Chem. Soc.* 2009;131:12868-12869.

12 Rachel A.; Subrahmanyam M.; Boule P. Comparison of Photocatalytic Efficiencies of TiO_2 in Suspended and Immobilised Form for the Photocatalytic Degradation of Nitrobenzenesulfonic Acids. *Appl. Catal. B: Environ.* 2002;37:301-308.

13 Chen P.; Gu L.; Xue X.; Li M.; Cao X. Engineering the Growth of TiO_2 Nanotube Arrays on Flexible Carbon Fibre Sheets. *Chem. Commun.* 2010;46:5906-5908.

14 Tatsuda N.; Itahara H.; Setoyama N.; Fukushima Y. Preparation of Titanium Dioxide/Activated Carbon Composites Using Supercritical Carbon Dioxide. *Carbon* 2005;43:2358-2365.

15 Zeng J.; Liu S.; Cai J.; Zhang L. TiO_2 Immobilized in Cellulose Matrix for Photocatalytic Degradation of Phenol under Weak Uv Light Irradiation. *J. Phys. Chem. C* 2010;114:7806-7811.

16 Naguib M.; Kurtoglu M.; Presser V.; Lu J.; Niu J.; Heon M.; Hultman L.; Gogotsi Y.; Barsoum M.W. Two-Dimensional Nanocrystals Produced by Exfoliation of Ti_3AlC_2. *Adv. Mater.* 2011;23:4248-4253.

17 Naguib M.; Mochalin V.N.; Barsoum M.W.; Gogotsi Y. Two-Dimensional Materials: 25th Anniversary Article: Mxenes: A New Family of Two-Dimensional Materials. *Adv. Mater.* 2014;26:982-982.

18 Lukatskaya M.R.; Mashtalir O.; Ren C.E.; Dall'Agnese Y.; Rozier P.; Taberna P.L.; Naguib M.; Simon P.; Barsoum M.W.; Gogotsi Y. Cation Intercalation and High Volumetric Capacitance of Two-Dimensional Titanium Carbide. *Science* 2013;341:1502-1505.

19 Ghidiu M.; Lukatskaya M.R.; Zhao M.Q.; Gogotsi Y.; Barsoum M.W. Conductive Two-Dimensional Titanium Carbide 'Clay' with High Volumetric Capacitance. *Nature* 2014;516:78-81.

20 Naguib M.; Mashtalir O.; Carle J.; Presser V.; Lu J.; Hultman L.; Gogotsi Y.; Barsoum M.W. Two-Dimensional Transition Metal Carbides. *ACS Nano* 2012;6:1322-1331.

21Peng Q.; Guo J.; Zhang Q.; Xiang J.; Liu B.; Zhou A.; Liu R.; Tian Y. Unique Lead Adsorption Behavior of Activated Hydroxyl Group in Two-Dimensional Titanium Carbide. *J. Am. Chem. Soc.* 2014;136:4113-4116.

22 Ghassemi H.; Harlow W.; Mashtalir O.; Beidaghi M.; Lukatskaya M.R.; Gogotsi Y.; Taheri M.L. In Situ Environmental Transmission Electron Microscopy Study of Oxidation of Two-Dimensional Ti_3C_2 and Formation of Carbon-Supported TiO_2. *J. Mater. Chem. A* 2014;2:14339-14343.

23 Naguib M.; Mashtalir O.; Lukatskaya M.R.; Dyatkin B.; Zhang C.; Presser V.; Gogotsi Y.; Barsoum M.W. One-Step Synthesis of Nanocrystalline Transition Metal Oxides on Thin Sheets of Disordered Graphitic Carbon by Oxidation of Mxenes. *Chem. Commun.* 2014;50:7420-7423.

24 Eames C.; Islam M.S. Ion Intercalation into Two-Dimensional Transition-Metal Carbides: Global Screening for New High-Capacity Battery Materials. *J. Am. Chem. Soc.* 2014;136:16270-16276.

25 Liu G.; Yang H.G.; Pan J.; Yang Y.Q.; Lu G.Q.; Cheng H. M. Titanium Dioxide Crystals with Tailored Facets. *Chem. Rev.* 2014;114:9559-9612.

26 Fang W.Q.; Gong X. Q.; Yang H.G. On the Unusual Properties of Anatase TiO_2 Exposed by Highly Reactive Facets. *J. Phys. Chem. Lett.* 2011;2:725-734.

27 Yang H.G.; Zeng H.C. Preparation of Hollow Anatase TiO_2 Nanospheres Via Ostwald Ripening. *J. Phys. Chem. B* 2004;108:3492-3495.

28 Song G.M.; Pei Y.T.; Sloof W.G.; Li S.B.; De Hosson J.T.M.; van der Zwaag S. Early Stages of Oxidation of Ti_3AlC_2 Ceramics. *Mater. Chem. Phys.* 2008;112:762-768.

29 Hosono E.; Fujihara S.; Kakiuchi K.; Imai H. Growth of Submicrometer-Scale Rectangular Parallelepiped Rutile TiO_2 Films in Aqueous $TiCl_3$ Solutions under Hydrothermal Conditions. *J. Am. Chem. Soc.* 2004;126:7790-7791.

30 Feng J.; Zeng H.C. Size-Controlled Growth of Co_3O_4 Nanocubes. *Chem. Mater.* 2003;15:2829-2835.

31 Tel H; Altaş Y; MS. T. Adsorption Characteristics and Separation of Cr(III) and Cr(VI) on Hydrous Titanium(IV) Oxide. *J. Hazard. Mater.* 2004;112:225-231.

32 Chang D.; Chen T.; Liu H.; Xi Y.; Qing C.; Xie Q.; Frost R.L. A New Approach to Prepare Zvi and Its Application in Removal of Cr(VI) from Aqueous Solution. *Chem. Eng. J.* 2014;244:264-272.

33 Lu J.; Liu H.; Zhao X.; Jefferson W.; Cheng F.; Qu J. Phosphate Removal from Water Using Freshly Formed Fe–Mn Binary Oxide: Adsorption Behaviors and Mechanisms. *Colloids Surf. Physicochem. Eng. Aspects* 2014;455:11-18.

34 Bourikas K.; Kordulis C.; Lycourghiotis A. Titanium Dioxide (Anatase and Rutile): Surface Chemistry, Liquid–Solid Interface Chemistry, and Scientific Synthesis of Supported Catalysts. *Chem. Rev.* 2014;114:9754-9823.

35 Bleam W.F.; McBride M.B. The Chemistry of Adsorbed Cu(II) and Mn(II) in Aqueous Titanium Dioxide Suspensions. *J. Colloid Interface Sci.* 1986;110:335-346.

36 Petsi T.; Panagiotou G.D.; Bourikas K.; Kordulis C.; Voyiatzis G.A.; Lycourghiotis A. Interfacial Impregnation Chemistry in the Synthesis of Chromium Catalysts Supported on Titania. *Chem. Cat. Chem* 2011;3:1072-1082.

37 Bourikas K.; Spanos N.; Lycourghiotis A. Advances in the Mechanism of Deposition of the CrO_4^{2-}, $HCrO_4^-$, and $Cr_2O_7^{2-}$ Species on the Surface of Titania Consisting of Anatase and Rutile. *Langmuir* 1997;13:435-444.

38 Spanos N.; Slavov S.; Kordulis C.; Lycourghiotis A. Mechanistic Aspects of the Deposition of the Cr(VI) Species on the Surface of TiO_2 and SiO_2. *Colloids Surf. Physicochem. Eng. Aspects* 1995;97:109-117.

39 Vassileva E.; Proinova I.; Hadjiivanov K. Solid-Phase Extraction of Heavy Metal Ions on a High Surface Area Titanium Dioxide. *Analyst* 1996;121:607-612.

40 Becke A.D.; Edgecombe K.E. A Simple Measure of Electron Localization in Atomic and Molecular Systems. *J. Chem. Phys.* 1990;92:5397-5403.

41 Ying Y.; Liu Y.; Wang X.; Mao Y.; Cao W.; Hu P.; Peng X. Two-Dimensional Titanium Carbide for Efficiently Reductive Removal of Highly Toxic Chromium(VI) from Water. *ACS Appl. Mater. Interfaces* 2015;7:1795-1803.

42 Kresse G.; Furthmüller J. Efficient Iterative Schemes for Ab Initio Total-Energy Calculations Using a Plane-Wave Basis Set. *Phys. Rev. B* 1996;54:11169-11186.

43 Perdew J.P.; Burke K.; Ernzerhof M. Generalized Gradient Approximation Made Simple. *Phys. Rev. Lett.* 1996;77:3865-3868.

44 Blöchl P.E. Projector Augmented-Wave Method. *Phys. Rev. B* 1994;50:17953-17979.

45 Monkhorst H.J.; Pack J.D. Special Points for Brillouin-Zone Integrations. *Phys. Rev. B* 1976;13:5188-5192.

46 Monkhorst H.J. Hartree-Fock Density of States for Extended Systems. *Phys. Rev. B* 1979;20:1504-1513.

Figure 1. Microstructural characterization. (a) SEM image of Al-removing MXene. (b) SEM image of analogous u-RTC composite prepared in (MXene-IPA-0.5EG)-1$FeCl_3$ for 12 h. (c) the local high magnification of (b). (d) and (e) TEM and high-resolution TEM images of rutile TiO_2, respectively. It reveals the u-RTC consists of (110) facets. (f) The represents Raman spectrum of analogous u-RTC composite.

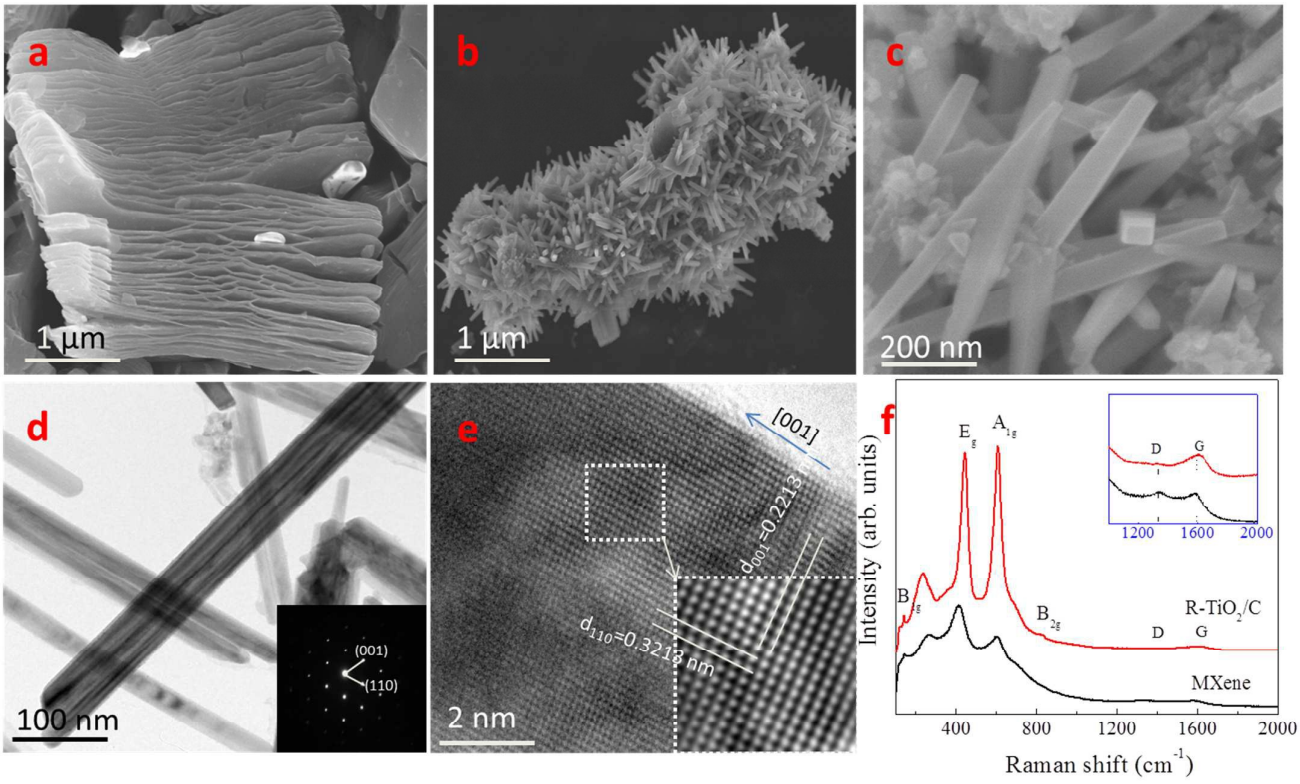

Figure 2. **Microstructural variation dependent on reaction time.** (a) SEM image of u-RTC prepared in (MXene-IPA-0.5EG)-1$FeCl_3$ for 1 h. (b) and (c) high-resolution TEM images of nanorod rutile TiO_2 and nano-cuboid anatase TiO_2. The SEM images of the samples at 200℃ for 12 h (d) and at 300℃for 24 h (e). (f) The effect of reaction time on the width and thickness of rutile TiO_2 in (MXene-IPA-0.5EG)-1$FeCl_3$ at 200℃, which is calculated based on 15 random measures by SEM observation.

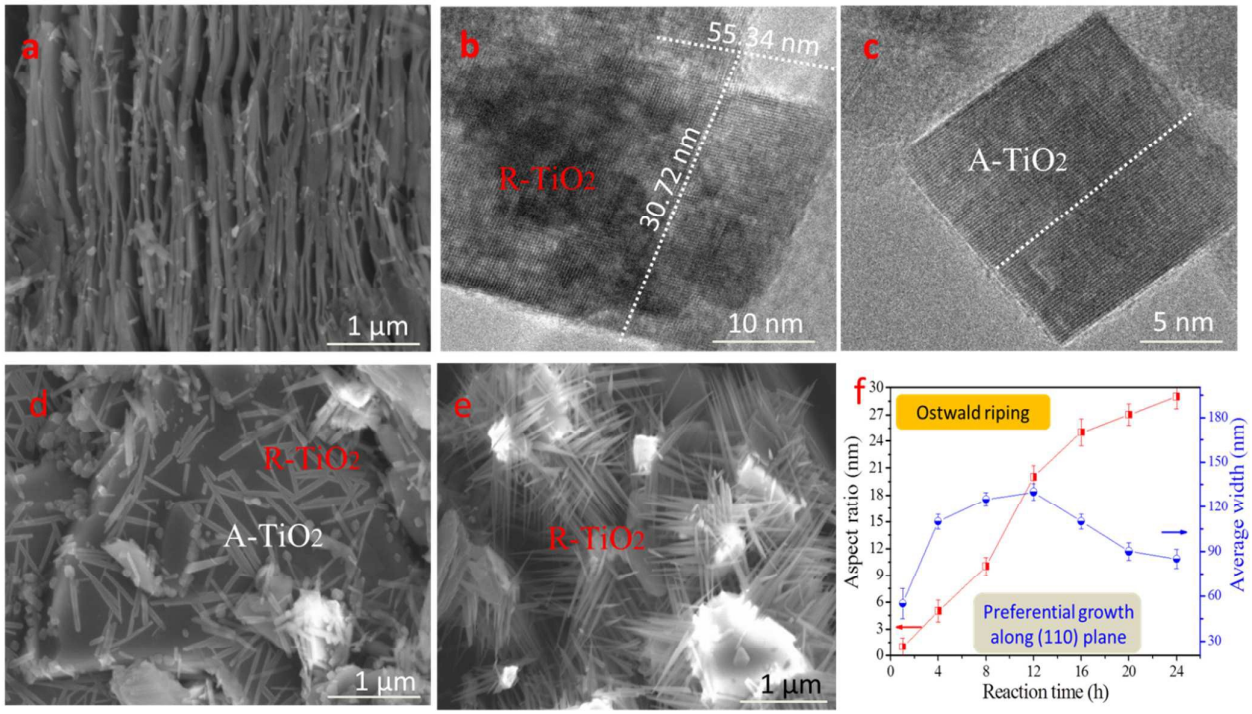

Figure 3. Cr(VI) sorption behavior. (a) Cr(VI) sorption performances onto the prepared l-ATC in (MXene-IPA)-0.5EG at 200 ℃ for 12 h, u-RTC and l-ATC in (MXene-IPA-0.5EG)-1$FeCl_3$ at 220 ℃ for 24 h, u-RTC in (MXene-IPA-0.5EG)-1$FeCl_3$ at 300 ℃ for 24 h and the primitive MXene. (Conditions: dose 0.5 g/L sorbents pH =5.8-6.4 at 298K with different Cr(VI) ion additions) (b) Solution pH effects for Cr(VI) sequestration onto u-RTC (conditions: dose 0.5 g/L sorbents, initial Cr(VI) =10 mg/L at 298K). (c) Sorption kinetic tests at various time interval (conditions: dose: 2 g/L, initial Cr(VI) =15 mg/L, 298K, pH =6.2-6.7). (d) Common anions influences for Cr(VI) uptake onto u-RTC (conditions: dose 0.5 g/L sorbents. pH=5.8-6.5 at room temperature).

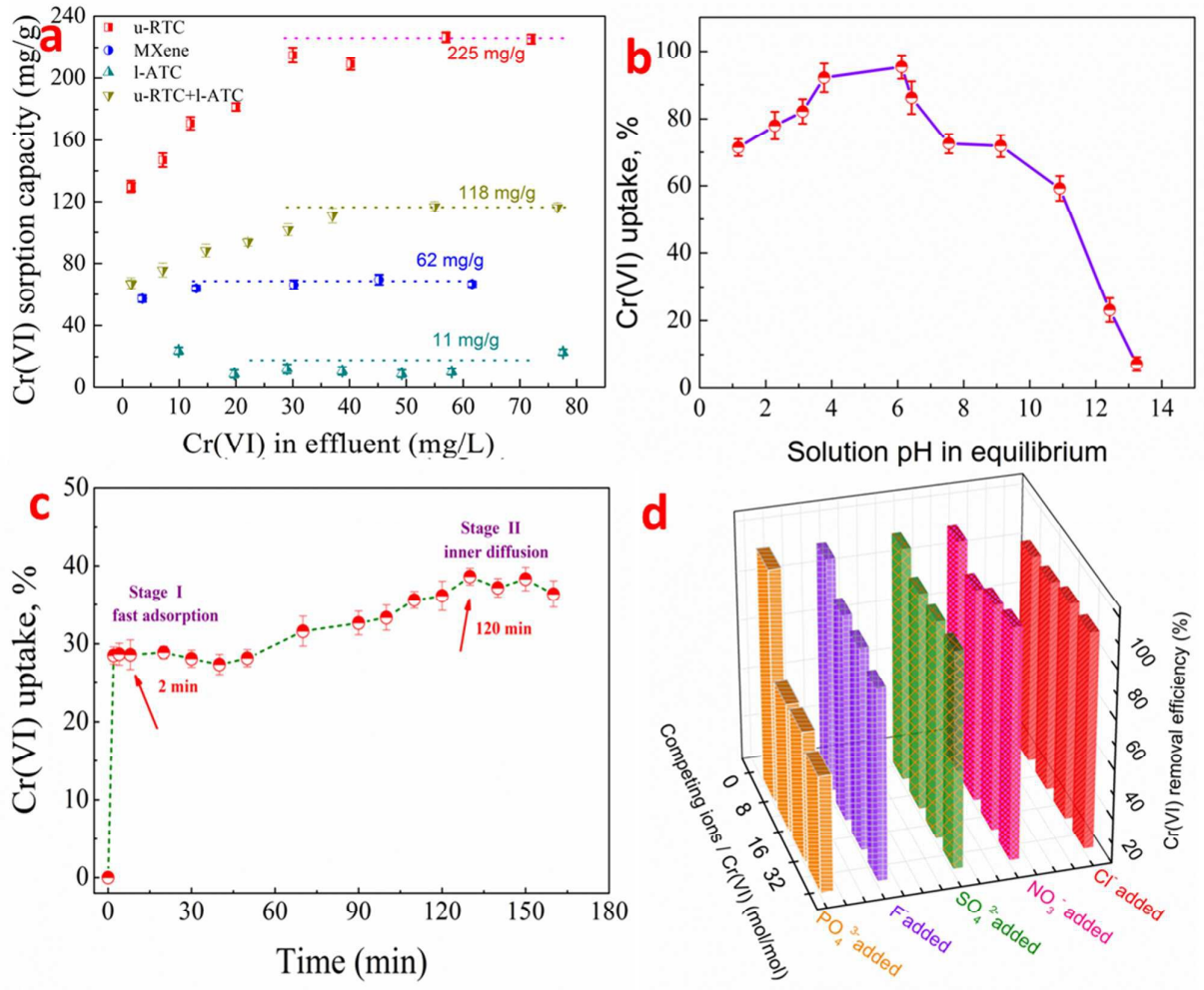

Figure 4 High-resolution XPS spectra of u-RTC at 300℃ for 24 h. a) XPS spectra of u-RTC before and after Cr(VI) uptake; b) Cr 2*p* spectra of Cr(VI)-adsorbed u-RTC and pure $K_2Cr_2O_7$ samples; c) O1*s* spectra of u-RTC; d)) O1*s* spectra of u-RTC with Cr(VI) loading.

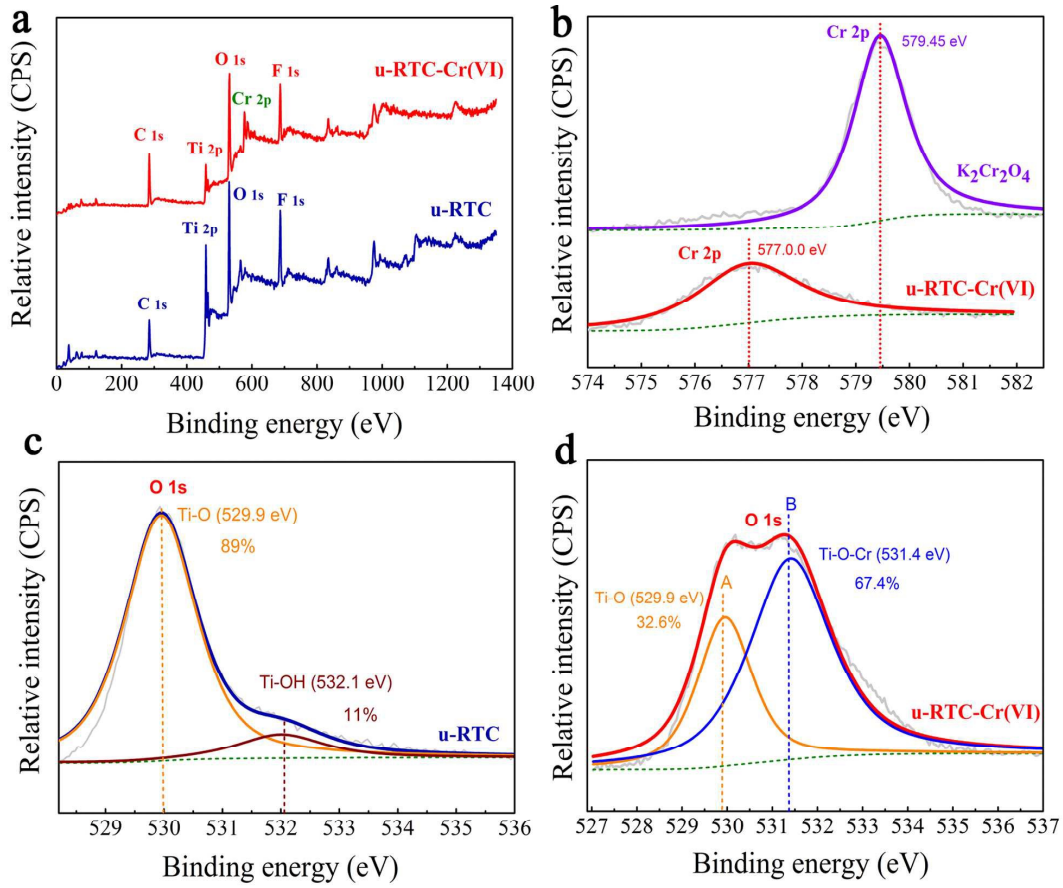

Figure 5 The applied evaluation onto u-RTC with feeding synthetic Cr(VI) contaminated waters (dose：2 g/L, initial Cr(VI) = 2 mg/L, SO_4^{2-}=Cl^-= NO_3^-=200 mg/L pH =5.5-6.8) .The right insert figure is sorption-regeneration cycles (regenerant: 5% NaOH solution at 298K)

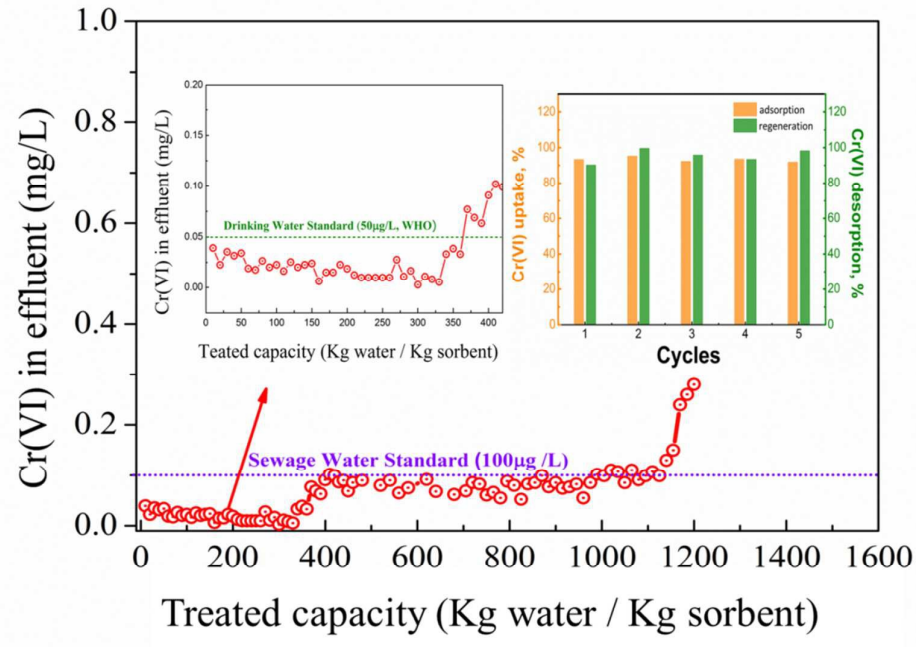

Figure 6 The typical sketch maps. a) The adsorption sketch map of CrO_4^{2-} (I-type), $HCrO_4^-$ (II-type), and $Cr_2O_7^{2-}$ (III-type) ions using the different adsorption structures of H_2CrO_4 and $H_2Cr_2O_7$ adsorption on rutile TiO_2 (110) surface, respectively. The sketch map of H_2O adsorption on different TiO_2 surfaces; b) R-TiO_2 (110); c) A-TiO_2 (101); d) A-TiO_2 (001).

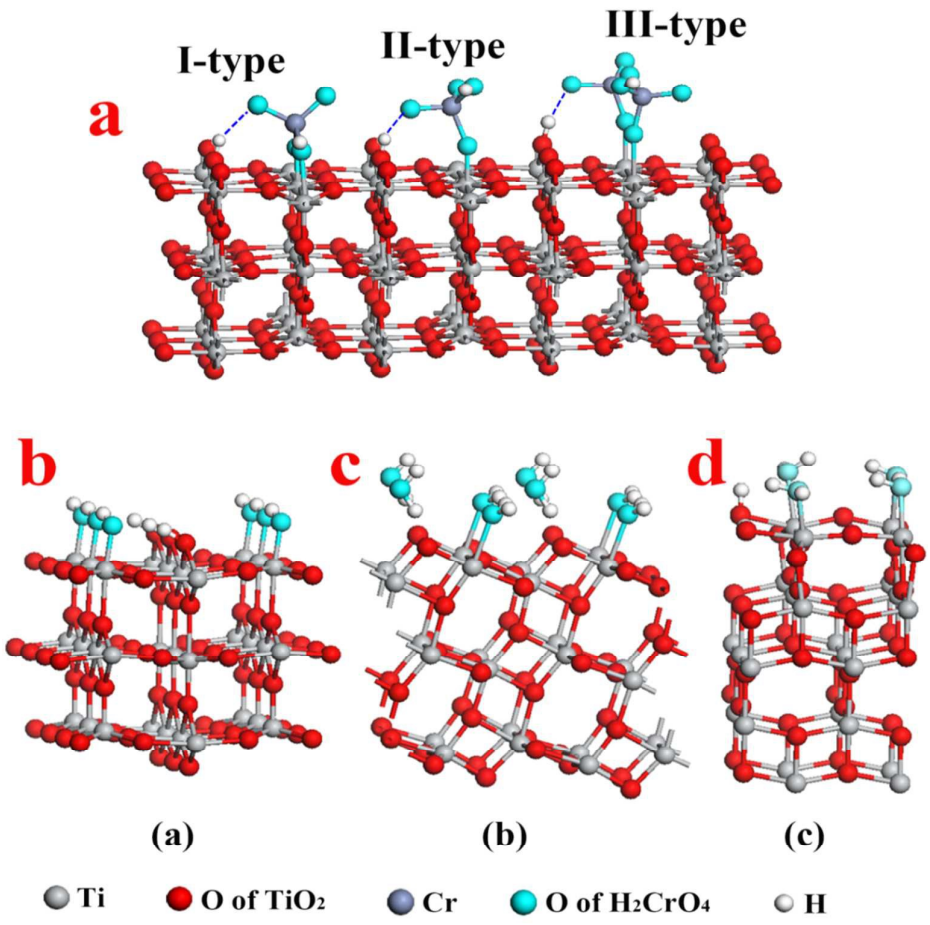

Figure 7 The average adsorption energies of H_2O, H_2CrO_4 and $H_2Cr_2O_7$ as three forms of CrO_4^{2-}, $HCrO_4^-$, and $Cr_2O_7^{2-}$ ions. (a) A-TiO_2 (101); (b) A-TiO_2 (001); (c) R-TiO_2 (110). (d) R-TiO_2 (101).The subscripts represent the number of H_2O on the surface. (e) The schematic maps of lattice planes for two different TiO_2 compounds

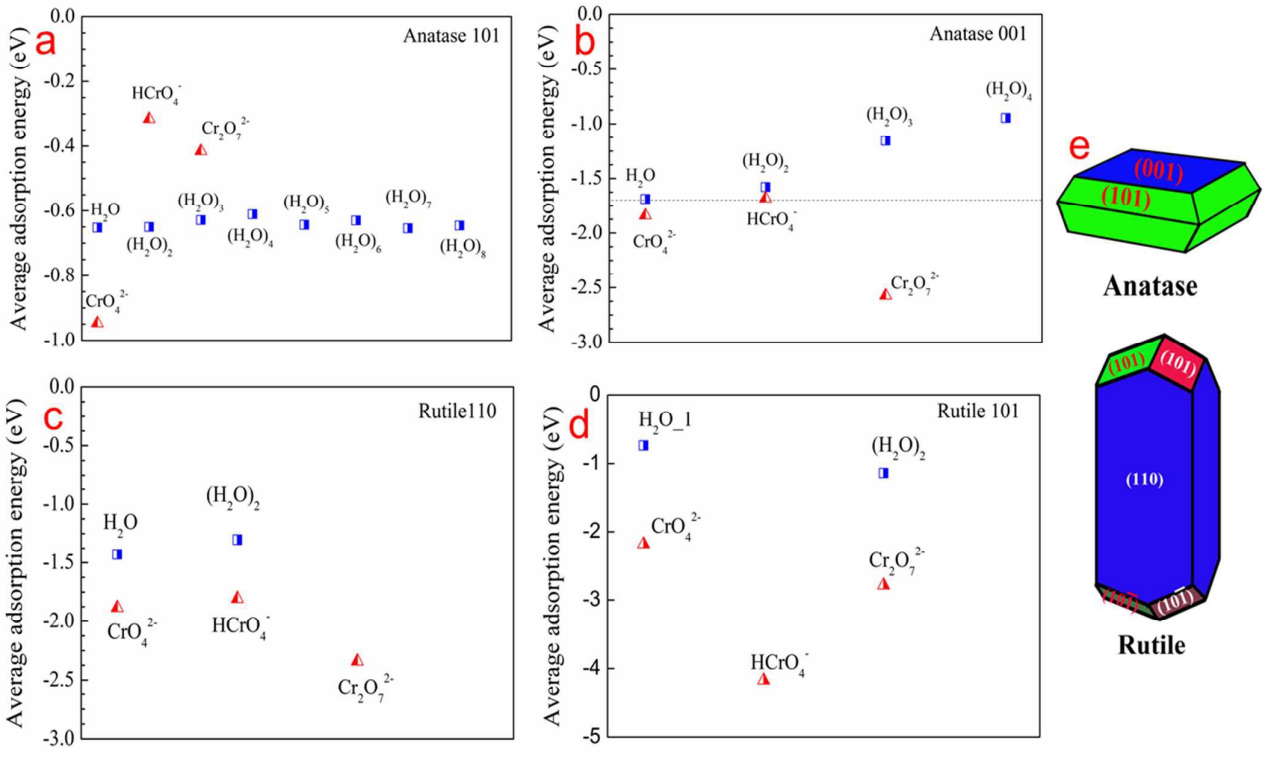

TOC figure

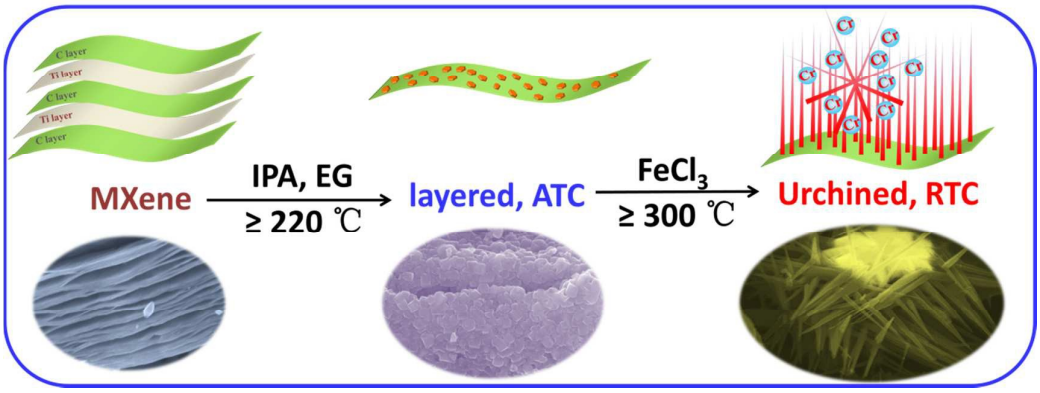

We fabricate a novel two-dimensional material by in-situ phase transformation of layered MXene with the induction of Fe(III) ion. This analogous urchined rutile TiO_2-C nanocomposite with a high amount of (110) activated facets, exhibits a high Cr(VI) adsorption ability of ~225 mg/g, which is the most highest value based on a simple adsorption mechanism due to the inhibition of H_2O molecule adsorption by bridging oxo groups. This method offers a simple and mild route to prepare different two-dimensional oxide-carbon based composites by tailoring solvent compositions, which can also be extended to self-assemble functional surfaces of other MXene derivatives.